Crustal thickness variations in the Aegean region and implications for the extension of continental crust

Lupei Zhu,[1] Brian J. Mitchell,[1] Nihal Akyol,[2] Ibrahim Cemen,[3] and Kivanc Kekovali[4]

Received 10 April 2005; revised 18 September 2005; accepted 5 October 2005; published 6 January 2006.

[1] We installed 5 broadband and 45 short-period temporary seismic stations, distributed partly as a dense, 100-km-long, N-S linear array and partly as a regional network, throughout the Menderes Massif of western Turkey in order to study crust-upper mantle structure and seismicity. In this study, we have combined teleseismic waveform data from these stations with data from several permanent seismic stations to determine crustal thickness variations in the Aegean region. Receiver function studies at seven broadband stations, using the H-κ stacking method, have yielded crustal thicknesses and V_p/V_s ratios over a broad region of the Aegean. A more detailed crustal image was obtained in the central Menderes Massif, where we applied common conversion point stacking to receiver functions obtained from the N-S linear array. The results show a general trend of westward crustal thinning from 36 km in central Anatolia to 28–30 km in the central Menderes Massif to 25 km beneath the Aegean Sea. The results also indicate that crustal thinning in the Aegean is not uniform in the N-S extensional direction. The crust is thinner in the central Menderes Massif (28–30 km of crustal thicknesses) and the Cycladic Massif (25–26 km) than in surrounding regions where crustal thicknesses are 32–34 km. The long-lived elevated Moho under the metamorphic core complexes suggests that the lower crust in the Aegean region is at least 3 times more viscous than that in the Basin and Range Province, where the Moho is much flatter.

Citation: Zhu, L., B. J. Mitchell, N. Akyol, I. Cemen, and K. Kekovali (2006), Crustal thickness variations in the Aegean region and implications for the extension of continental crust, *J. Geophys. Res.*, *111*, B01301, doi:10.1029/2005JB003770.

1. Introduction

[2] The Aegean region comprises the Aegean Sea, western Turkey, and mainland Greece (Figure 1). It experienced a series of continental collisions from the Late Cretaceous to the Eocene. Extension probably started as early as the late Oligocene and was widespread by the late Miocene [e.g., *Hetzel and Reischmann*, 1996; *Gautier et al.*, 1999; *Lips et al.*, 2001; *Catlos and Cemen*, 2005]. It is currently undergoing some of the most active continental extension in the world. N-S extension rates estimated from seismicity and GPS measurements range between 30 and 110 mm/yr [*Jackson and McKenzie*, 1988; *McClusky et al.*, 2000; *Nyst and Thatcher*, 2004]. Postcollisional extension in the region caused the exhumation of several Alpine metamorphic belts (metamorphic core complexes), where high-grade metamorphic rocks originating in the middle to lower crust are exposed at the surface. These belts are termed the Menderes, Crete, Cycladic, and Kazdag massifs (Figure 1). The timing and cause of the extension are still controversial, and many models, including those based upon orogenic collapse [e.g., *Dewey*, 1988], subducting slab rollback [e.g., *McKenzie*, 1978; *Le Pichon and Angelier*, 1979; *Royden*, 1993], and westward extrusion of the Anatolian block [e.g., *Dewey and Sengor*, 1979; *Cemen et al.*, 1999], have been proposed.

[3] The principal strains obtained from summing earthquake moment tensors indicate that the N-S extension is largely accompanied by vertical thinning, with very little E-W shortening [*Jackson and McKenzie*, 1988]. *Makris* [1975] and *Makris and Vees* [1977], using seismic refraction and gravity data, found that crustal thickness is 22–32 km beneath the Aegean Sea and 40–50 km beneath mainland Greece and Turkey. Assuming that the latter represents crust before extension, *McKenzie* [1978] estimated that the Aegean crust has been stretched by a factor of 2 since the late Miocene (~5 Ma). This stretching factor agrees with the accumulated vertical strain predicted by the measured seismic strain rate [*Jackson and McKenzie*, 1988]. It therefore seems likely that the entire crust, and probably also the lithosphere, has deformed coherently.

[4] Recent studies based on GPS measurements over the past decade [e.g., *McClusky et al.*, 2000; *Nyst and Thatcher*, 2004], however, have revealed a more complicated picture of contemporary deformation in the Aegean. The deformation is not uniform but is concentrated in zones separating a few near-rigid blocks (microplates). *McClusky et al.* [2000]

[1]Department of Earth and Atmospheric Sciences, Saint Louis University, Saint Louis, Missouri, USA.
[2]Department of Geophysics, Faculty of Engineering, Dokuz Eylül University, Buca-Izmir, Turkey.
[3]School of Geology, Oklahoma State University, Stillwater, Oklahoma, USA.
[4]Kandilli Observatory and Earthquake Research Institute, Bogazici University, Istanbul, Turkey.

0148-0227/06/2005JB003770$09.00

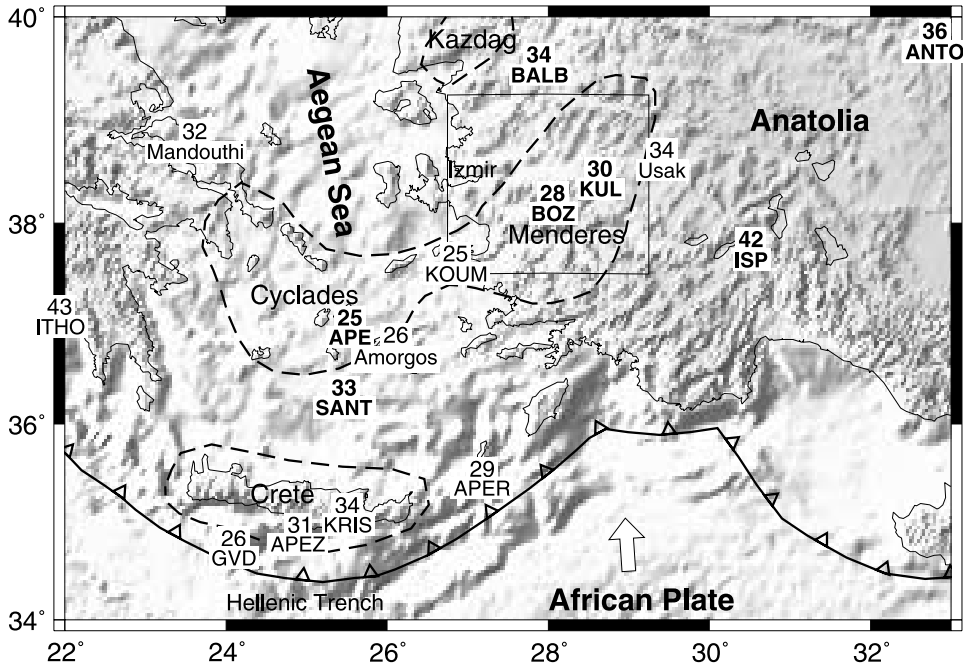

Figure 1. Distribution of the metamorphic core complexes in the Aegean region (dashed lines). Numbers indicate crustal thicknesses in km determined in this study (boldface) and in previous studies; see text for details. The rectangle outlines the study area of the 2002–2003 Western Anatolia Seismic Recording Experiment shown in Figure 2.

found that the central and southern Aegean (the south Aegean microplate) moves coherently toward the SW at 30 mm/yr relative to Eurasia, and the motion is accommodated by strike slip and extension in the north Aegean and N-S extension in western Turkey. *Nyst and Thatcher* [2004] suggested that present-day Aegean deformation is due to relative motions of four microplates: central Greece, the Sea of Marmara, the south Aegean, and Anatolia. Strain rates across microplate boundaries are 1 to 2 orders of magnitude larger than rates within internally deforming zones, which are 30–50 nstrain/yr.

[5] It should be pointed out that before the 1990s only a few crustal thickness measurements were available in the Aegean region. Most were obtained from seismic refraction profiling [e.g., *Makris*, 1975; *Makris and Vees*, 1977] and suffered limitations imposed by lateral structural variation and the trade-offs between crustal thickness and velocity. Inversion of gravity data can produce crustal thickness maps with much better coverage, as shown by *Tsokas and Hansen* [1997] and *Tirel et al.* [2004] for Greece and the Aegean Sea. However, results from gravity data are inherently nonunique and are affected by density variations both within the crust and in the mantle. Recently, with increases in the number of modern broadband seismic stations in the region and advances in data analysis techniques, several crustal thickness measurements using the teleseismic receiver function technique have been reported. *Saunders et al.* [1998] used seismic waveform data from two temporary arrays near Kula (KUL) and Usak in western Turkey and found that crustal thickness varies between 29 and 34 km, as compared to 38 km beneath station ANTO farther east (Figure 1). *Van der Meijde et al.* [2003] estimated crustal thicknesses beneath 15 broadband stations throughout a broader region of the Mediterranean. Three of the stations are in the Aegean area, and data from them yielded crustal thicknesses that vary from 25 km beneath station KOUM in the Aegean Sea to 29 km beneath station APER near the Hellenic trench to 43 km beneath station ITHO in Greece (Figure 1). *Li et al.* [2003] used broadband stations on the islands of Crete, Santorini (SANT), Naxos (APE), and Samos (KOUM) to construct receiver function images of the crust and upper mantle in the Hellenic subduction zone. They found crustal thicknesses of 25–32 km in the central Aegean Sea. The Moho lies between 31 and 39 km beneath the island of Crete. However, these results are far from certain, judging from their receiver functions which do not show Moho *Ps* (*P*-to-*S* converted wave) clearly and are complicated by intracrustal discontinuities and the subducting slab. Overall, crustal thickness measurements in the Aegean region are too sparse to reveal details of thickness variations or to correlate thicknesses with amounts of extension mapped by geology. Part of the limitation on spatial resolution is due to the large station spacings of permanent seismic stations in the region.

[6] In this study, we used teleseismic waveform data from a seismic recording experiment in western Turkey and permanent seismic stations in the Aegean Sea and Turkey to determine crustal thicknesses in the region. We first briefly describe the 2002–2003 Western Anatolia Seismic Recording Experiment, followed by a description of the two crustal thickness estimation methods used. The first method, namely, the H-κ stacking method [*Zhu and Kanamori*, 2000], is applied to teleseismic receiver functions of isolated broadband stations and yields estimates of both crustal thickness (H) and V_p/V_s ratio (κ). The second method, common conversion point (CCP) stacking [*Kosarev et al.*,

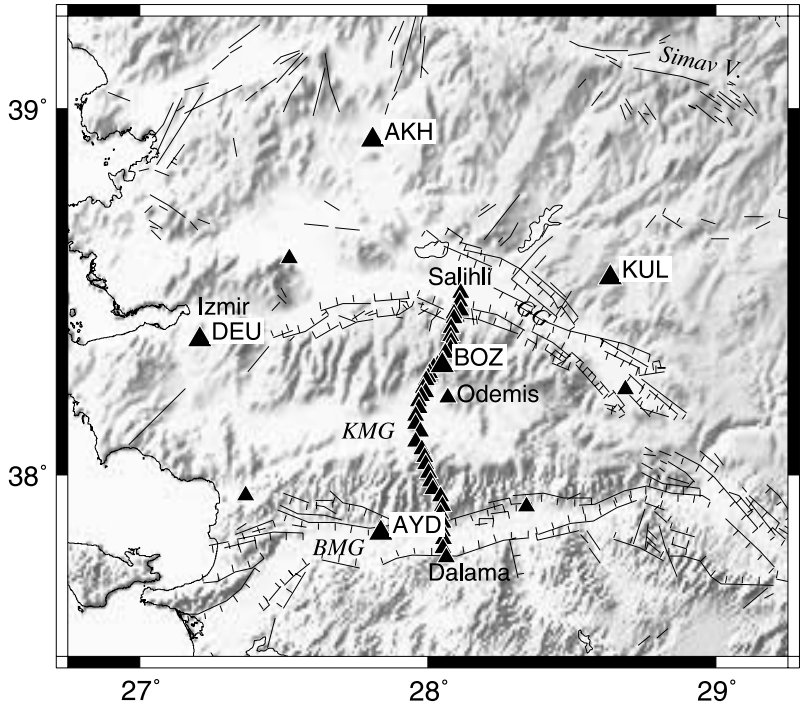

Figure 2. Temporary seismic stations (solid triangles) deployed during the 2002–2003 Western Anatolia Seismic Recording Experiment. The names of broadband stations appear next to the symbols. BMG, Buyuk Menderes Graben; GG, Gediz Graben; KMG, Kucuk Menderes Graben.

1999; *Zhu*, 2000, 2002], is applied to closely spaced stations of a linear array and produces crustal images of layering and lateral variations of crustal structure. We combine our crustal thickness results with those of previous studies to infer variations in crustal thickness in the Aegean region and to discuss their implications for the extension of continental lithosphere and exhumation of metamorphic core complexes.

2. The 2002–2003 Western Anatolia Seismic Recording Experiment

[7] Between November 2002 and October 2003, seismologists from Saint Louis University and Dokuz Eylül University in Izmir, Turkey, deployed 50 seismic stations in western Turkey (Figure 2). We used 5 STS-2 broadband and 24 Mark L-22 short-period (2 Hz) three-component sensors. Twenty of the short-period instruments were first deployed for 6 months along a 50-km-long N-S line between Salihli and Odemis in the central Menderes Massif. They were redeployed in May 2003 to extend the line southward an additional 50 km from Odemis to Dalama. This design provided a 100-km-long N-S profile with a station spacing of 3–4 km. The profile traversed two prominent E-W trending grabens in western Turkey: the Buyuk Menderes Graben (BMG) and the Kucuk Menderes Graben (KMG). The remaining four short-period and five broadband instruments were installed to form a regional network over a 150×150 km^2 area surrounding the linear array. All stations recorded ground motion continuously at a rate of 40 samples per second. They were visited every 1 or 2 months for maintenance and data download. The data were sent to Saint Louis University where they were converted to Standard for the Exchange of Earthquake Data (SEED) format, checked for quality control, and organized in a database managed with Program for Array Seismic Studies of the Continental Lithosphere (PASSCAL) software. In total, we collected more than 120 Gb of compressed waveform data, which is 93% of the amount of data that should have been collected with no downtime for any station. The data set has been permanently archived at the Incorporated Research Institutions for Seismology (IRIS) data management center with a designated network code of XE-02 and will be available for general access by the end of 2005.

3. Methods

3.1. H-κ Stacking

[8] A receiver function determined from a seismic station recording represents the response of local crustal structure to a near vertically impinging plane wave. The dominant signal following the direct P wave on the radial receiver function is the P-to-S converted wave (Ps) from the Moho discontinuity. The conversion point lies within 10 km in horizontal distance from the station. The arrival time difference t_{Ps} between Ps and P on a receiver function can be used to estimate the crustal thickness H beneath the station. Because the differential travel time between S and P waves is used, the thickness estimate is not sensitive to the crustal P wave velocity, V_p, as much as to the crustal V_p/V_s ratio κ. This trade-off between H and κ can be reduced significantly by adding multiply converted phases, namely, $PpPs$ and $PpSs + PsPs$ [*Zhu*, 1993; *Zandt et al.*, 1995]. *Zhu and Kanamori* [2000] developed a stacking algorithm which sums the ampli-

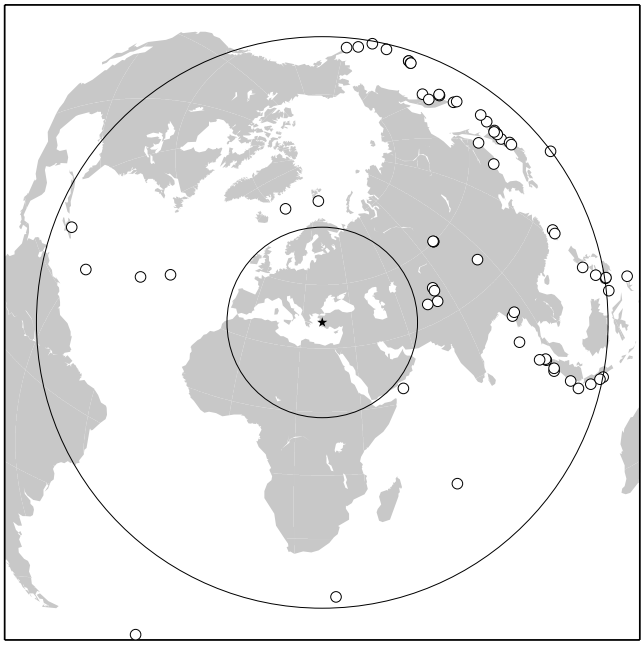

Figure 3. Equidistance projection of locations of teleseismic events used in this study. The two circles represent epicentral distance of 30° and 90°.

tudes of receiver functions at the predicted arrival times of these phases for different crustal thicknesses H and κ. This transforms the time domain receiver functions directly into the H-κ domain without the need to identify these converted phases and to pick their arrival times. The best estimations of H and κ are found when the three phases are stacked coherently. The technique works well for isolated broadband stations on hard rock where the absence of shallow sediments precludes P-to-S reverberations in the sedimentary layer from obscuring Moho-converted phases.

[9] In the original method of *Zhu and Kanamori* [2000] the amplitudes of the three phases are stacked as a weighted sum. The primary converted phase Ps is usually given a large weight of 60 to 70%, and the first multiple, $PpPs$, is given a weight of 20–30%. The scheme is based on signal-to-noise ratios of those phases and is subjective to some degree. We recently improved the method by separating the procedure into two steps. In the first step, all receiver functions are stacked after having been corrected to a common incident angle. The "best" t_{Ps} is then obtained at the maximum amplitude in the stack. Although the move out correction must assume values for crustal velocities V_p and V_s, it is found that their influence on t_{Ps} is almost negligible. In the second step, once t_{Ps} is found, all receiver functions are stacked again along the $PpPs$ arrival time curves predicted by different κ values with the thickness H determined from the t_{Ps}. The maximum in the second stack gives the "best" κ estimate. The uncertainties of t_{Ps} and κ are calculated on the basis of the variances of the stacks and the sharpness at the maxima. An advantage of the modified algorithm, other than avoiding weighting among difference phases, is that when κ is not constrained by a $PpPs$ phase, one can still get an important measurement of t_{Ps} and use it to estimate crustal thickness by assuming a crustal V_p/V_s ratio.

3.2. CCP Stacking

[10] The primary purpose of the dense 100-km-long N-S linear array is to image crustal structure beneath the central Menderes Massif. The profile and important tectonic features in the region appear in Figure 2. *Dueker and Sheehan* [1997] used the idea of common midpoint (CMP) stacking in reflection seismology and developed a receiver function CMP stacking method by geographically binning receiver functions according to their piercing points at certain depth. All receiver functions in the same bin are stacked after being corrected for incidence angle move out. A shortcoming of the method is that it does not account for change in location of the piercing point with depth due to the slope of the ray path. *Kosarev et al.* [1999] and *Zhu* [2000] improved the CMP stacking method and developed the receiver function common conversion point (CCP) stacking technique. The algorithm consists of two steps: back projection and stacking. First, every amplitude on a radial receiver function following the direct P is assumed to be generated by a single P-to-S conversion along the ray path. The amplitude is projected to the conversion point using a background velocity model. Second, after back projecting all receiver functions the crustal volume is divided into bins of designated size, and all amplitudes in the same bin are stacked to produce a structural image. The amplitude of each pixel represents the impedance contrast at that location so that the image delineates various interfaces such as the Moho discontinuity.

[11] The lateral resolution of a CCP image is determined by the size of the Fresnel zone of the teleseismic P wave, which varies with depth z as $\sqrt{\lambda z}$, where λ is the wavelength. For a typical 1-Hz receiver function the Fresnel zone is a few kilometers in the upper crust and ~10 km near the Moho depth. In our CCP stacking, we use the size of the Fresnel zone as the horizontal size of the stacking bin. The vertical resolution of the image is generally limited by uncertainties in crustal seismic velocities, ranging from less than 1 km for a 3% uncertainty in crustal P wave velocity to 2 km for a 3% uncertainty in crustal V_p/V_s ratio [*Zhu and Kanamori*, 2000].

4. Data and Results

[12] In the 11-month recording period, 65 teleseismic earthquakes in the distance range of 30–98 were recorded with good signal-to-noise ratios by the temporary seismic network. They covered most of the northern back azimuthal range (Figure 3). Their P wave waveforms were used to calculate teleseismic receiver functions at each station. We first removed instrument responses from the raw data and applied band-pass filtering to the waveforms to enhance the signal-to-noise ratio. For broadband stations the filtering was applied between 0.1 and 2 Hz where teleseismic body wave energy is the strongest. Removing instrument responses for short-period stations is especially necessary because their responses fall off rapidly when signal frequencies are lower than 2 Hz. All short-period instrument responses were obtained using an on-site calibration method [*Rodgers et al.*, 1995]. Because of the inferior sensitivity of

Table 1. Station Locations and Crustal Thickness Estimates

Network[a]/Station	Latitude/Longitude/Elevation	Number of Receiver Functions	t_{Ps},[b] s	V_p/V_s	H,[c] km
XE/BOZ	38.30/28.05/1216	38	3.67 ± 0.24	1.773 ± 0.041	28.3 ± 1.9
XE/KUL	38.54/28.63/700	25	3.81 ± 0.34	1.752 ± 0.041	30.1 ± 2.7
GE/APE	37.07/25.53/620	37	3.26 ± 0.28	1.759 ± 0.046	25.5 ± 2.2
GE/ISP	37.84/30.51/1100	100	5.36 ± 0.37	1.756 ± 0.027	42.2 ± 2.9
GE/SANT	36.37/25.46/540	66	4.05 ± 0.43	1.730 ± 0.054	33.0 ± 3.5
IU/ANTO	39.87/32.79/883	93	4.83 ± 0.31	1.800 ± 0.063	35.9 ± 2.3
KO/BALB	39.64/27.88/120	23	4.32 ± 0.33	–	33.8 ± 2.6

[a]XE, our temporary network; GE, GEOForschungsNetz; IU, IRIS/USGS Network; KO, Kandilli Observatory, Istanbul, Turkey.
[b]For incident angle corresponding to a ray parameter of 0.06 s/km.
[c]Crustal thicknesses estimated from t_{Ps} and V_p/V_s assuming a crustal P velocity of 6.2 km/s.

short-period instruments to long-period ground motion and the microseismic noise that peaks at ~0.2–0.3 Hz, we applied a slightly different band-pass filtering of 0.2–2 Hz to short-period waveforms.

[13] We computed receiver functions using a time domain iterative deconvolution algorithm [*Kikuchi and Kanamori*, 1982; *Ligorria and Ammon*, 1999]. After deconvolution of 100 iterations we applied additional Gaussian low-pass filtering to suppress noise above 1 Hz in the receiver functions. We also processed teleseismic waveform data between 2002 and 2004 from three permanent broadband stations in Turkey (BALB, ISP, and ANTO) and two in the Aegean Sea (APE and SANT). Their locations and network affiliations are listed in Table 1. We excluded stations on the islands of Crete and Gavdos that are close to the Hellenic trench to avoid complications caused by the subducting slab. All receiver functions were visually inspected by sorting them according to back azimuth and incident angle and comparing each of them with neighboring receiver functions. Receiver functions with anomalous shapes or amplitudes on either radial or tangential component were discarded. We obtained a total of 803 receiver functions for short-period stations and 536 receiver functions for broadband stations.

[14] For each broadband station, receiver functions having similar incident angles (i.e., ray parameters) were averaged. Figure 4 shows such averaged receiver functions for stations BOZ, KUL, AYD, and BALB. For stations BOZ and KUL the Moho *P*-to-*S* converted phase *Ps* and its multiple *PpPs* can be clearly identified. The high quality of receiver functions for those two stations is largely due to the excellent site conditions since they were installed on basement rock. By contrast, the other three temporary broadband stations (AKH, AYD, and DEU) were located in sedimentary basins, and their receiver functions are overwhelmed by reverberations in the low-velocity sedimentary layer. An example is shown in Figure 4 for station AYD in the Buyuk Menderes Graben. The large-amplitude phase immediately after the direct P (at $t = 0$ s) is the *P*-to-*S* conversion at the bottom of the basin, and the following positive and negative amplitudes in the first 15 s are the basin reverberations. The reverberations obscure the Moho-converted phases and prevent determination of crustal thicknesses beneath those stations.

[15] By applying the H-κ stacking method to the receiver functions of station BOZ and KUL we found the crustal thickness beneath BOZ to be 28.3 ± 1.9 km with an average crustal V_p/V_s ratio of 1.773 ± 0.041, and we found the crustal thickness beneath KUL to be 30.1 ± 2.7 km with an average V_p/V_s ratio of 1.752 ± 0.041. Because of the clear Moho *Ps* and *PpPs* phases in those receiver functions we consider these crustal parameters to be well constrained. The arrival times of *Ps* and *PpPs* predicted by the estimated crustal thickness and V_p/V_s ratio were compared with times of the receiver function waveforms and found to be in good agreement with the data (Figure 4).

[16] Crustal thickness and V_p/V_s ratio results for all seven broadband stations are listed in Table 1. All stations show clear Moho *Ps* phases in their receiver functions (Figure 5). Six of them have identifiable *PpPs* phases, thus providing constraints on both crustal thicknesses and V_p/V_s ratios. Receiver functions of station BALB do not show a recognizable *PpPs* phase in the time window corresponding to crustal V_p/V_s ratios from 1.5 to 2.0 (Figures 4 and 5). The absence of the multiply converted phase could be due to high attenuation of that phase because it traverses a low-Q crust three times. A more plausible explanation is that lateral heterogeneity of crustal structure, including undulations of Moho and surface topography, scatters *PpPs*. Because that phase travels large lateral distances in the crust and is reflected from the free surface before being converted to an *S* wave at the Moho, lateral heterogeneities affect the arrival times and amplitudes of *PpPs* more than they do *Ps*. The crustal thickness beneath BALB was therefore estimated on the basis of only the *Ps* arrival time using an averaged V_p/V_s ratio of 1.76.

[17] *Saunders et al.* [1998] obtained crustal velocity beneath stations KUL and ANTO using a receiver function inversion method with a fixed V_p/V_s ratio of 1.732. Their crustal thickness estimate beneath KUL is the same as ours. They found a crustal thickness of 38 km beneath ANTO, which compares favorably with our estimated thickness of 36.2 ± 2.3 km. The small difference can be attributed to differences in V_p/V_s ratio for the two studies. Our crustal thickness estimates for stations APE and SANT in the central Aegean Sea also agree with those of *Li et al.* [2003].

[18] Receiver functions of stations along the N-S profile were stacked using the CCP method. The crustal volume sampled by these receiver functions is about 30 km wide along the 100-km-long profile. We used a two-layer crustal velocity model as the background velocity model to trace teleseismic ray paths in the volume and to compute *P*-to-*S* conversion points at different depths. The P wave velocity is 6.0 km/s in the upper 15 km and 6.2 km/s in the lower 15 km of the crust. These velocities are consistent with the P wave velocity model from local earthquake travel times

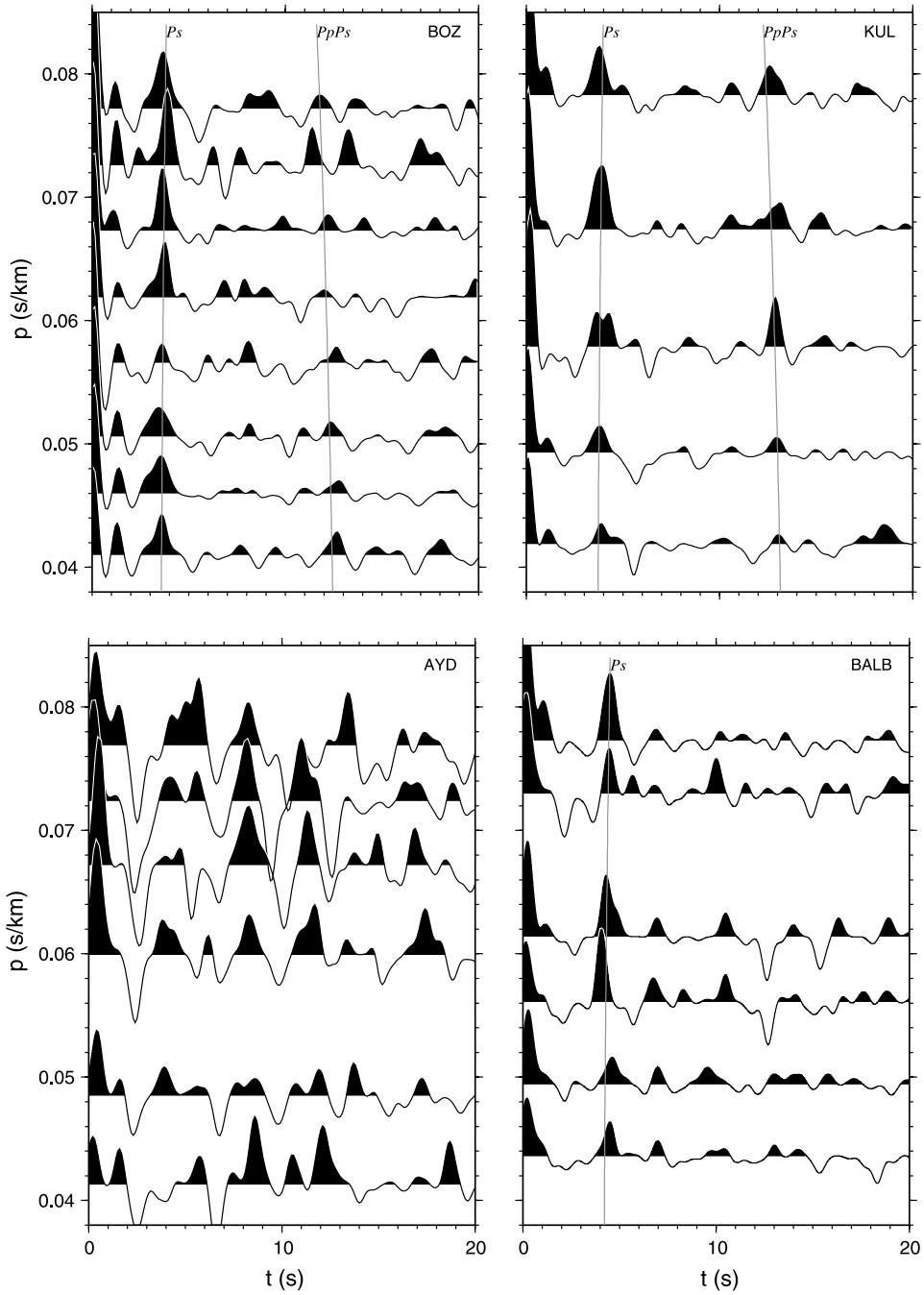

Figure 4. Receiver functions for stations BOZ, KUL, AYD, and BALB as a function of ray parameter. Also shown are arrival times of the Moho *Ps* and its multiple *PpPs* predicted by the determined crustal thickness and V_p/V_s ratio when available.

(N. Akyol et al., Crustal structure and local seismicity in western Anatolia, submitted to *Geophysical Journal International*, 2005). The crustal V_p/V_s ratio is set at 1.76, which is determined from the above broadband receiver functions for BOZ and KUL. For stations located in sedimentary basins we embedded a sedimentary layer, 4.0 km/s in *P* velocity and 2.0 km/s in *S* velocity, in the upper crustal layer. The thickness of the sedimentary layer varies from station to station and is determined iteratively from the CCP image until the input and output thicknesses agree (see below).

[19] The CCP image along the profile is shown in Figure 6. The Moho can be seen clearly as a continuous band of positive *P*-to-*S* conversion amplitudes between depths of 26 and 28 km. It shows that within the central Menderes Massif the Moho is relatively flat. The other continuous features with large positive amplitudes in the image are close to the surface and are prominent beneath the grabens (BMG, KMG, and Gediz Graben (GG)). We interpret them as bands of *P*-to-*S* converted energy at the interface between the low-velocity sedimentary layer and the basement. The sediment thicknesses vary from less than

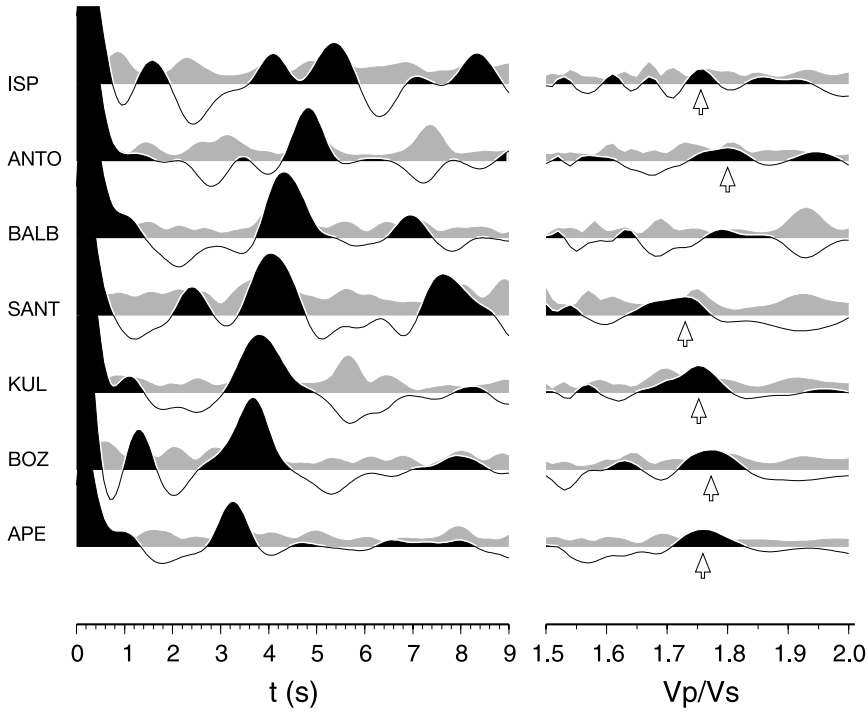

Figure 5. (left) Stacked receiver functions of all seven broadband stations arranged in order of (top to bottom) decreasing Moho *Ps* delays. Receiver functions were corrected to a ray parameter of 0.06 s/km before stacking. The 1σ standard deviations are shown in gray. (right) Stacked receiver functions along predicted arrival times of *PpPs* phase using different crustal V_p/V_s ratios. Arrow points to where the "best" ratio is picked.

1 to 3 km. There is no intracrustal interface that can be coherently detected in the CCP image. Several short positive bands in the middle to lower crust occur beneath sedimentary basins and are most likely to be basin reverberations mapped to deeper depths by the CCP.

[20] The crustal thicknesses determined using the receiver function method in this study and previous studies by *Saunders et al.* [1998] (station Usak), *Van der Meijde et al.* [2003] (stations APER, ITHO, and KOUM), and *Li et al.* [2003] (stations on the island of Crete) are shown in Figure 1. We also included estimated crustal thicknesses from a seismic refraction line from Mandouthi to Amorgos in the Aegean Sea [*Makris and Vees*, 1977]. The results show a general trend of westward crustal thinning from 36 km in central Anatolia to 28–34 km in western Anatolia to 25–33 km beneath the Aegean Sea. The thinning is, however, not uniform in the N-S extension direction. It seems that significant crustal thinning has occurred beneath the central Menderes Massif, where crustal thicknesses are 28–30 km compared to 34 km under stations BALB and Usak outside the massif and the Cycladic Massif, where the crustal thicknesses are 25–26 km compared to 33 km under station SANT outside the massif. We discuss these results and their implications in section 5.

5. Discussion

5.1. Stretching Factor of the Aegean Lithosphere

[21] From analyzing geophysical and geological data in the Aegean region, *McKenzie* [1978] developed a simple model of lithosphere extension that has only one parameter,

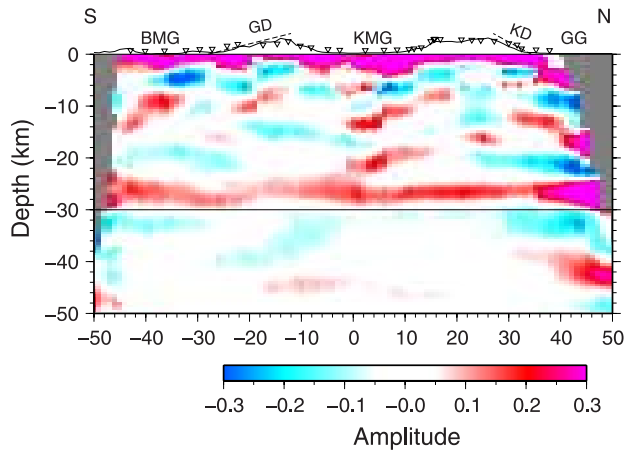

Figure 6. Common conversion point crustal image along the N-S profile across the central Menderes Massif. Red represents positive *P*-to-*S* converted amplitudes and normally indicates sharp increase in acoustic impedance with depth. The Moho is the continuous band between 26 and 28 km in depth. The strong positive amplitudes near the surface are produced by the large impedance contrast between sediments and basement rock. Dashed lines represent the Guney Detachment (GD) and the Kuzey Detachment (KD). There is no vertical exaggeration except that the surface topography is amplified by a factor of 2.

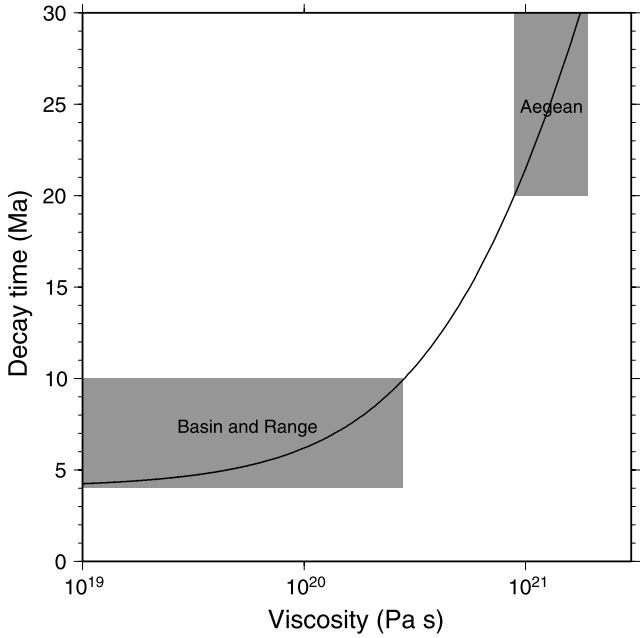

Figure 7. Moho topography decay time as a function of lower crustal viscosity, following the two-layer model of *McKenzie et al.* [2000]. The thickness of the lower crust is 10 km, and the wavelength of Moho topography is 200 km. The viscosity of the mantle lithosphere is fixed as 10^{22} Pa/s. The decay times for the Aegean and the Basin and Range Province are estimated using their current Moho topography amplitudes and an initial amplitude of 10 km 30 Myr ago; see text for details.

the stretching factor β. He estimated that the Aegean lithosphere has been stretched by a factor of 2 since the late Miocene of ~5 Myr ago. This was largely based on early reports of a thick crust (close to 50 km) in mainland Greece and Turkey and very thin crust (22–32 km) beneath the Aegean Sea. The thickest crust (42 km) among the stations that we analyzed is beneath station ISP (Figure 1). A similar crustal thickness of 43 km under station ITHO in Greece was obtained by *Van der Meijde et al.* [2003] (Figure 1). However, station ISP is located in the so-called Isparta Angle area where the Hellenic and Cyprus arcs intersect. Similarly, station ITHO is in close proximity to the western Hellenic trench. It is therefore reasonable to suspect that the crust there has been thickened by subduction-related compression and shortening following earlier extension. If we assume that the 36-km-thick crust beneath station ANTO in central Anatolia represents original crust before the extension, we calculate that the crust has been stretched by a factor of 1.1 outside the metamorphic core complexes in the Aegean region, by a factor of 1.2 in the Menderes Massif, and by a factor of 1.4 in the Cycladic Massif. Those estimates are in good agreement with the moderate stretching factors of 1.2–1.4 estimated by *Angelier et al.* [1982] on the basis of a simple stretching model.

[22] Our 33-km crustal thickness under station SANT south of the Cycladic Massif is much larger than either the 15-km thickness reported earlier for the crust beneath the Cretan Sea from a short seismic refraction profile [*Bohnhoff et al.*, 2001] or the 22-km thickness obtained from gravity data [*Tirel et al.*, 2004]. Receiver functions for station SANT show clear Moho *P*-to-*S* converted phases so that both the crustal thickness and V_p/V_s ratio are well constrained. Whether or not the values are representative of the crust beneath the entire Cretan Sea is uncertain. On the other hand, the seismic refraction line used by *Bohnhoff et al.* [2001] might be too short to rule out a deeper Moho. The result of gravity data inversion is inherently nonunique and depends on how corrections for the subducting slab are implemented. Similar ambiguity exists for crustal thickness beneath the northern Aegean Sea. *Horasan et al.* [2002] obtained a thickness of 33 km from modeling regional seismic waveforms. Inversion of gravity data suggested a thinner crust of 22 km thick [*Tirel et al.*, 2004]. It may be possible to resolve these controversies in the future by employing long seismic refraction lines, perhaps including ocean bottom stations.

5.2. Comparison of the Aegean Region and the Basin and Range

[23] It has long been recognized that extension of continents can occur in either "distributed" or "localized" mode. In the localized mode, extension is concentrated in a rift system of closely spaced high-angle normal faults, such as that in the East African Rift. Both the crust and mantle lithosphere beneath the rift thin substantially more than do those in surrounding regions. In the distributed mode the brittle upper crust accommodates deformation by many normal faults, each with a limited amount of slip but distributed over a wide area. The more viscous underlying lower crust and mantle lithosphere are assumed to undergo uniform ductile deformation with the same total amount of extension. An additional mode termed the "metamorphic core complex mode" was proposed by *Buck* [1991] and is characterized by concentrated upper crustal extension with lower crustal thinning over a broad area. Unlike the distributed mode, extension in the upper crust is mainly accommodated by large displacement on a single low-angle detachment fault that separates the core complex and the upper plate rock. Examples of the metamorphic core complex mode are the Basin and Range Province of the western United States and the Aegean region. The manner in which the lower crust and the mantle lithosphere beneath metamorphic core complexes respond to the extension is presently unclear. For the Basin and Range, results of seismic reflection surveys show no appreciable Moho topography [e.g., *Gans*, 1987] even though geological estimates of extension vary between 15 and 300%. This suggests that the lower crust is so weak that it can flow laterally on a short timescale to smooth the Moho topography induced by extension. The Aegean region seems different from the Basin and Range Province, as shown by the crustal thicknesses in Figure 1, because the Moho is elevated by 4–8 km beneath metamorphic core complexes compared to areas outside.

[24] *McKenzie et al.* [2000] investigated characteristics of lower crustal flow using a simplified model of a fluid layer over a fluid half-space. They found that density and viscosity contrasts affect the length scales and timescales over which flow occurs. Figure 7 shows Moho topography decay time as a function of lower crustal viscosity in their model. The viscosity of the mantle lithosphere is fixed as

10^{22} Pa/s, and the thickness of the lower crust is 10 km. We used a wavelength of Moho topography of 200 km based on the spacing of metamorphic core complexes in the Aegean (Figure 1). We estimated decay times for the Aegean region and the Basin and Range Province using their current Moho topography amplitudes and assuming that the initial Moho relief was 10 km when the metamorphic core complexes were exhumed. The age of the core complexes in the Aegean is about 30 ± 10 Ma [*Hetzel and Reischmann*, 1996; *Gautier et al.*, 1999; *Lips et al.*, 2001; *Catlos and Cemen*, 2005]. Core complexes in the Basin and Range Province are of similar age [e.g., *Wernicke*, 1985]. Moho topography amplitudes in the Aegean region range between 4 and 8 km, which yields a lower bound of decay time of ~20 Myr. Seismic studies indicate that the Basin and Range is devoid of any appreciable Moho topography [e.g., *Gans*, 1987]. Assuming it is less than 1 km gives an upper bound of ~10 Myr for decay time there. Moho decay times in the two regions were used to estimate viscosities of the lower crust (Figure 7). The estimates indicate that the lower crustal viscosity in the Aegean is at least 3 times larger than in the Basin and Range. A strong Aegean lower crust is consistent with GPS results that show most of the Aegean moves as a group of near-rigid blocks [*McClusky et al.*, 2000; *Nyst and Thatcher*, 2004].

5.3. Formation of Metamorphic Core Complexes

[25] The Moho topography found in the Aegean region also sheds light on the mechanism of continental extension and associated metamorphic core complex development. These processes have been controversial, especially with respect to the role of low-angle detachment faults. Since the early 1980s two end-member models have emerged on the basis of field-oriented research in the southern Basin and Range Province, where the continental crust has experienced pervasive Cenozoic extension. The first model is usually referred to as the simple shear model [e.g., *Wernicke*, 1981; *Spencer*, 1984; *Wernicke*, 1985]. In this model a large-displacement low-angle normal fault initiates at a primary "breakaway," and movement of the hanging wall causes isostatic uplift of the footwall as extension occurs. The second model, often referred to as the flexural rotation/rolling hinge model [e.g., *Buck*, 1988; *Wernicke and Axen*, 1988; *Axen and Bartley*, 1997; *Gessner et al.*, 2001; *Seyitoglu et al.*, 2002], starts with a deep-seated normal fault of high angle. As the footwall is uplifted and flexed upward in isostatic response to unloading, the shallow part of the fault is rotated to a low-dip angle and becomes inactive. The footwall is progressively exhumed as the fault bend migrates in the direction of the hanging wall like a rolling hinge.

[26] Note that the two models require entirely different normal fault geometries and lower crustal structures. The simple shear model requires a large-scale low-angle detachment and smoothly varying Moho, but the flexural rotation/rolling hinge model requires high-angle normal faults penetrating the entire crust and producing a rapid Moho variation parallel to the extension direction. Although the Moho topography decays with time because of crustal relaxation, as discussed in section 5.2, the decay time is a function of wavelength λ. For linear viscosity the decay time of Moho topography is inversely proportional to wavelength when $\lambda \ll 2\pi h$, where h is the thickness of the viscous lower crust [see *McKenzie*, 1978]. Therefore the sharp Moho steps produced by high-angle normal faults should decay more slowly than longer wavelengths comparable to $2\pi h$. The CCP crustal image in Figure 6 shows that the Moho beneath the N-S linear array is relatively flat between depths of 26 and 28 km. This profile was, however, located entirely within the central Menderes metamorphic core complex. The crustal thickness results from isolated broadband stations in the Aegean region (Figure 1) show that Moho increases in depth by 4–8 km over a lateral distance of less than 100 km from the metamorphic core complexes to the upper plates, e.g., station APE (25 km) versus SANT (33 km) and station KUL (30 km) versus Usak (34 km). Other studies have shown that the Moho is elevated beneath several large normal faults in the northern Aegean Sea [e.g., *Makris and Stobbe*, 1984; *Taymaz et al.*, 1991]. The number of available measurements is, however, still small, and more work is needed to discriminate one model from the other on the basis of Moho depth variations. It will be especially important to extend the linear profile to the north and south so that they cross the boundaries of the Menderes Massif. In that way we can determine if there is an abrupt change in Moho depth across those boundaries.

6. Conclusions

[27] In summary, we have combined teleseismic waveform data from a temporary seismic network in western Turkey and permanent seismic stations to determine crustal thickness variations in the Aegean region. The results show a general trend of westward crustal thinning from 36 km in central Anatolia to 28–30 km in the central Menderes Massif to 25 km beneath the Aegean Sea. Our results also indicate that crustal thinning in the Aegean is not uniform in the N-S extensional direction. It is greater in the metamorphic belts that comprise the Menderes Massif, where crustal thicknesses are 28–30 km, and the Cycladic Massif, where they are 25–26 km, than in surrounding regions, where they are 32–34 km. The long-lived elevated Moho under the metamorphic core complexes suggests that the lower crust in the Aegean region is at least 3 times more viscous than that in the Basin and Range Province, where the Moho discontinuity is relatively flat.

[28] **Acknowledgments.** Constructive reviews by Simon Lloyd, an anonymous reviewer, and a JGR Associate Editor significantly improved the manuscript. Participants of the 2002–2003 Western Anatolia Seismic Recording Experiment include Mike Fort of IRIS/PASSCAL and M. Ali Danisman, Hasan Sozbilir, Oguz Demir, Zulfikar Erhan, Adem Somer, and Emre Timur of DEU. We are grateful to numerous village officials and residents in our study area for their support. The fieldwork was funded by NSF Office of International Programs under grant INT-0217493 and by the Scientific and Technical Research Council of Turkey (TUBITAK) under grant YDABAG 102Y015. Waveform data of the GEOFON and IRIS/USGS stations used in this study were downloaded from the IRIS/DMC. L.Z. was partially supported by a Saint Louis University summer research award.

References

Angelier, J., N. Lyberis, X. Le Pichon, E. Barrier, and P. Huchon (1982), The tectonic development of the Hellenic arc and the Sea of Crete: A synthesis, *Tectonophysics*, *86*, 159–196.

Axen, G. J., and J. Bartley (1997), Field tests of rolling hinges: Existence, mechanical types and implications for extensional tectonics, *J. Geophys. Res.*, *102*, 20,515–20,537.

Bohnhoff, M., J. Makris, D. Papanikolaou, and G. Stavrakakis (2001), Crustal investigation of the Hellenic subduction zone using wide aperture seismic data, *Tectonophysics*, *343*, 239–262.

Buck, W. R. (1988), Flexural rotation of normal faults, *Tectonics*, *7*, 959–973.

Buck, W. R. (1991), Modes of continental lithosphere extension, *J. Geophys. Res.*, *96*, 20,161–20,178.

Catlos, E. J., and I. Cemen (2005), Monazite ages and rapid exhumation of the Menderes Massif, western Turkey, *Int. J. Earth Sci.*, *94*, 204–217.

Cemen, I., M. C. Goncuoglu, and K. Dirik (1999), Structural evolution of the Tuzgolu Basin in central Anatolia, Turkey, *J. Geol.*, *107*, 693–706.

Dewey, J. F. (1988), Extensional collapse of orogens, *Tectonics*, *7*, 1123–1139.

Dewey, J. F., and A. M. C. Sengor (1979), Aegean and surrounding regions: Complex multiple and continuum tectonics in a convergent zone, *Geol. Soc. Am. Bull.*, *90*, 84–92.

Dueker, K., and A. Sheehan (1997), Mantle discontinuity structure from midpoint stacks of converted *P* to *S* waves across the Yellowstone hotspot track, *J. Geophys. Res.*, *102*, 8313–8327.

Gans, P. B. (1987), An open-system, two layer crustal stretching model for the eastern Great Basin, *Tectonics*, *6*, 1–12.

Gautier, P., J. Brun, R. Moriceau, D. Sokoutis, J. Martinod, and L. Jolivet (1999), Timing, kinematics and cause of Aegean extension: A scenario based on a comparison with simple analogue experiments, *Tectonophysics*, *315*, 31–72.

Gessner, K., U. Ring, C. W. Passchier, C. Johnson, R. Hetzel, and T. Gungor (2001), An active bivergent rolling-hinge detachment system: Central Menderes metamorphic core complex in western Turkey, *Geology*, *29*, 611–614.

Hetzel, R., and T. Reischmann (1996), Intrusion age of Pan-African augen gneisses in the southern Menderes Massif and the age of cooling after Alpine ductile extensional deformation, *Geol. Mag*, *133*, 565–572.

Horasan, G., L. Gulen, A. Pinar, D. Kalafat, N. Ozel, H. S. Kuleli, and A. M. Isikara (2002), Lithospheric structure of the Marmara and Aegean regions, western Turkey, *Bull. Seismol. Soc. Am.*, *92*, 322–329.

Jackson, J., and D. McKenzie (1988), The relationship between plate motions and seismic moment tensors and rates of active deformation in the Mediterranean and Middle East, *Geophys. J.*, *93*, 45–73.

Kikuchi, M., and H. Kanamori (1982), Inversion of complex body waves, *Bull. Seismol. Soc. Am.*, *72*, 491.

Kosarev, G., R. Kind, S. Sobolev, X. Yuan, W. Hanka, and S. Oreshin (1992), Seismic evidence for a detached Indian lithospheric mantle beneath Tibet, *Science*, *283*(5406), 1306–1309.

Le Pichon, X., and J. Angelier (1979), The Aegean arc and trench system: A key to the neotectonic evolution of the eastern Mediterranean area, *Tectonophysics*, *60*, 1–42.

Li, X., G. Bock, A. Vafidis, R. Kind, H. P. Harjes, W. Hanka, K. Wylegalla, M. van der Meijde, and X. Yuan (2003), Receiver function study of the Hellenic subduction zone: Imaging crustal thickness variations and the oceanic Moho of the descending African lithosphere, *Geophys. J. Int.*, *155*, 733–748.

Ligorria, J. P., and C. J. Ammon (1999), Iterative deconvolution and receiver-function estimation, *Bull. Seismol. Soc. Am.*, *89*, 1395–1400.

Lips, A. L. W., D. Cassard, H. Sozbilir, H. Yilmaz, and J. R. Wijbrans (2001), Multistage exhumation of the Menderes Massif, western Anatolia (Turkey), *Int. J. Earth Sci.*, *89*, 781–792.

Makris, J. (1975), Crustal structure of the Aegean Sea and the Hellenides, obtained from geophysical survey, *J. Geophys.*, *41*, 441–443.

Makris, J., and C. Stobbe (1984), Physical properties and state of the crust and upper mantle of the eastern Mediterranean Sea deduced from geophysical data, *Mar. Geol.*, *55*, 347–363.

Makris, J., and R. Vees (1977), Crustal structure of the central Aegean Sea and the islands of Evvia and Crete, Greece, obtained by refraction experiments, *J. Geophys. Res.*, *42*, 329–341.

McClusky, S., S. Balassanian, A. Barka, C. Demir, and S. Ergintav (2000), Global positioning system constraints on the plate kinematics and dynamics, *J. Geophys. Res.*, *105*, 5695–5791.

McKenzie, D. (1978), Active tectonics of the Alpine-Himalayan belt: The Aegean Sea and surrounding regions, *Geophys. J. R. Astron. Soc.*, *55*, 217–254.

McKenzie, D., F. Nimmo, J. A. Jackson, P. B. Gans, and E. L. Miller (2000), Characteristics and consequences of flow in the lower crust, *J. Geophys. Res.*, *105*, 11,029–11,046.

Nyst, M., and W. Thatcher (2004), New constraints on the active tectonic deformation of the Aegean, *J. Geophys. Res.*, *109*, B11406, doi:10.1029/2003JB002830.

Rodgers, P. W., A. M. Martin, M. C. Robertson, M. M. Hsu, and D. B. Harris (1995), Signal-coil calibration of electromagnetic seismometers, *Bull. Seismol. Soc. Am.*, *85*, 845–850.

Royden, L. (1993), Evolution of retreating subduction boundaries formed during the continental collision, *Tectonics*, *12*, 629–638.

Saunders, P., K. Priestley, and T. Taymaz (1998), Variation in the crustal structure beneath western Turkey, *Geophys. J. Int.*, *134*, 373–389.

Seyitoglu, G., O. Tekeli, I. Cemen, S. Sen, and V. Isk (2002), The role of the flexural rotation/rolling hinge model in the tectonic evolution of the Alasehir Graben, western Turkey, *Geol. Mag.*, *139*, 15–26.

Spencer, J. E. (1984), The role of tectonic denudation in the warping and uplift of low-angle normal faults, *Geology*, *12*, 95–98.

Taymaz, T., J. Jackson, and D. McKenzie (1991), Active tectonics of the north and central Aegean Sea, *Geophys. J. Int.*, *106*, 433–490.

Tirel, C., F. Gueydan, C. Tiberi, and J.-P. Brun (2004), Aegean crustal thickness inferred from gravity inversion, Geodynamical implications, *Earth Planet. Sci. Lett.*, *228*, 267–280.

Tsokas, G. N., and R. O. Hansen (1997), Study of the crustal thickness and the subducting lithosphere in Greece from gravity data, *J. Geophys. Res.*, *102*, 20,585–20,597.

Van der Meijde, M., S. Van der Lee, and D. Giardini (2003), Crustal structure beneath broad-band seismic stations in the Mediterranean region, *Geophys. J. Int.*, *152*, 729–739.

Wernicke, B. (1981), Low-angle normal faulting in the Basin and Range Province: Nappe tectonics in an extending orogen, *Nature*, *291*, 645–648.

Wernicke, B. (1985), Uniform-sense normal-simple shear of the continental lithosphere, *Can. J. Earth Sci.*, *22*, 108–125.

Wernicke, B., and G. J. Axen (1988), On the role of isostasy in the evolution of normal fault systems, *Geology*, *16*, 848–851.

Zandt, G., S. C. Myers, and T. C. Wallace (1995), Crust and mantle structure across the Basin and Range-Colorado Plateau boundary at 37°N latitude and implications for Cenozoic extensional mechanism, *J. Geophys. Res.*, *100*, 10,529–10,548.

Zhu, L. (1993), Estimation of crustal thickness and V_p/V_s ratio beneath the Tibetan Plateau from teleseismic converted waves, *Eos Trans. AGU*, *74*(16), Spring Meet. Suppl., 202.

Zhu, L. (2000), Crustal structure across the San Andreas Fault, southern California from teleseismic converted waves, *Earth Planet. Sci. Lett.*, *179*, 183–190.

Zhu, L. (2002), Deformation in the lower crust and downward extent of the San Andreas Fault as revealed by teleseismic waveforms, *Earth Planets Space*, *54*, 1005–1010.

Zhu, L., and H. Kanamori (2000), Moho depth variation in southern California from teleseismic receiver functions, *J. Geophys. Res.*, *105*, 2969–2980.

N. Akyol, Department of Geophysics, Faculty of Engineering, Dokuz Eylül University, Kaynaklar Campus, 35160 Buca-Izmir, Turkey.

I. Cemen, School of Geology, Oklahoma State University, Stillwater, OK 74078-0451, USA.

K. Kekovali, Kandilli Observatory and Earthquake Research Institute, National Earthquake Monitoring Center, Bogazici University, 34684 Cengelkoy-Istanbul, Turkey.

B. J. Mitchell and L. Zhu, Department of Earth and Atmospheric Sciences, Saint Louis University, 3507 Laclede Avenue, Saint Louis, MO 63103, USA. (lupei@eas.slu.edu)